Research Square

Preprints are preliminary reports that have not undergone peer review.
They should not be considered conclusive, used to inform clinical practice,
or referenced by the media as validated information.

Numerical simulation and monitoring experiment of liquid injection diffusion range in ionic rare earth ores

Gang Min

mingang2012@cdut.edu.cn

Key Laboratory of Earth Exploration and Information Technology of Ministry of Education, Chengdu University of Technology

Zhihao Zhang

Key Laboratory of Earth Exploration and Information Technology of Ministry of Education, Chengdu University of Technology

Yang Yu

Ningxia Hui Autonomous Region Coal Geology Bureau

Wenyu Li

Key Laboratory of Earth Exploration and Information Technology of Ministry of Education, Chengdu University of Technology

Hai Qin

Key Laboratory of Earth Exploration and Information Technology of Ministry of Education, Chengdu University of Technology

Rongbo Shu

Institute of Multipurpose Utilization of Mineral Resources

Research Article

Keywords: Ionic rare earth ore, Time-lapse resistivity tomography, Seepage numerical simulation, Resistivity structure, monitoring experiment

Posted Date: March 25th, 2026

DOI: https://doi.org/10.21203/rs.3.rs-9048823/v1

License: This work is licensed under a Creative Commons Attribution 4.0 International License.
Read Full License

Additional Declarations: No competing interests reported.

Numerical simulation and monitoring experiment of liquid injection diffusion range in ionic rare earth ores

Gang Min[1*], Zhihao Zhang[1], Yang Yu[3], Wenyu Li[1], Qin Hai[1], Rongbo Shu[2*]

(1. Key Laboratory of Earth Exploration and Information Technology of Ministry of Education, Chengdu University of Technology, Chengdu 610059, China; 2.Institute of Multipurpose Utilization of Mineral Resources, Chengdu 610041, China; 3. Ningxia Hui Autonomous Region Coal Geology Bureau, Yinchuan, 750021, China)

Abstract: Currently, in-situ leaching is the predominant method for extracting ionic rare earth ores. However, this technique still faces persistent challenges such as low resource utilization efficiency and environmental issues including water and soil contamination. Clarifying the diffusion characteristics of the leach liquid is crucial for addressing these problems. Geophysical methods, particularly conductive electrical techniques, have been widely employed to monitor the diffusion range of the leach liquid. Nevertheless, these methods suffer from limitations such as operational complexity, high costs, and poor timeliness. To overcome these drawbacks, this study first utilizes numerical simulation to determine the influence range of liquid injection, and subsequently evaluates the effectiveness of the high-density resistivity method in delineating its diffusion extent. Based on the deep structural characteristics of a rare earth mine in Fujian, China, identified through high-density resistivity method, a suitable site was selected for a comparative experiment. The experiment compared time-lapse resistivity tomography monitoring with seepage numerical simulations of liquid injection faced actual geological model, and the results demonstrated good consistency in the diffusion ranges identified by both methods. Through theoretical analysis and comparative monitoring results, this study proposes that the integrated approach of "detailed deep structure investigation & seepage numerical simulation of liquid injection" can effectively characterize the diffusion behavior of the leach liquor. This provides theoretical support for the precise placement of injection wells and the design of anti-seepage systems in ionic rare earth mining. contributing to improved mineral recovery rates and reduced environmental pollution from liquid injection.

Keywords: Ionic rare earth ore; Time-lapse resistivity tomography; Seepage numerical simulation; Resistivity structure; monitoring experiment

Corresponding author：Gang Min, male, doctor, born in 1983, mingang2012@cdut.edu.cn

Highlights:

1. Both seepage simulation and electrical resistivity tomography (ERT) confirm a significant decrease in resistivity within the liquid injection diffusion zone.

2. The spatial structural parameters of the geological model control both the diffusion range of the injected liquid and the anisotropy of the resistivity model.

3. Combining detailed deep structure investigation with seepage numerical simulation can effectively characterize the diffusion behavior of the liquid injection.

1. Introduction

Rare earth ores are hailed as "industrial gold" due to their exceptional physical and chemical properties, and they hold irreplaceable application value in critical sectors such as national defense, energy and chemical industries, and aerospace (Wei et al. 2024). The ion-adsorption type heavy rare earth ores developed in South China, are particularly precious, accounting for over 70% of global reserves and supplying 90% of the world's market (Tang et al. 2024; Zhou et al. 2020). At present, the in-situ leaching is the primary mining method for ionic rare earth ores (Kang et al., 2024), however, this mining method still faces challenges such as the generally low recovery rate (only 30%-50%), and soil and water pollution caused by extensive mining practices (Chen 2019; Xie et al. 2018). The core of the in-situ leaching process lies in two critical steps: "solution injection" and "solution recovery", and the construction of the recovery system and its efficiency represent a technological bottleneck in the industry (Wang et al. 2025), which is closely related to the unclear flow paths of the leach liquid due to factors such as uneven weathering, development of structural fractures, and basement topography (Wang et al. 2015). Therefore, there is an urgent need to accurately explore the deep structures of mining areas and understand the diffusion characteristics of liquid injection, which will provide theoretical support for the precise placement of injection wells and recovery tunnels, as well as targeted anti-seepage engineering measures.

Time-lapse electrical resistivity tomography (ERT) has been widely used for dynamic monitoring of deep fluid movements, however, its application in long-term monitoring within large-scale, topographically complex regions faces challenges such as high implementation difficulty, elevated costs, and poor timeliness (Min et al. 2022; Li et al. 2024; Netto et al. 2025). With onging advances in computational technology, many researchers have turned to sophisticated geotechnical numerical simulation software to conduct simulations and analyses of scientific issues such as seepage field evolution and solute transport, achieving a series of research outcomes (Wen et al. 2025). Nevertheless, when performing seepage numerical simulations in practical engineering projects, the accurate construction of geological structural models is a crucial prerequisite. Geophysical methods, recognized for their strong penetrative capability, high efficiency, and low economic costs, offer significant technical advantages and application potential in the investigation of deep geological structures (Luo et al. 2023; Yang, 2020; Chen et al. 2023).

Based on the above background, this study first demonstrates the feasibility of using high-density ERT to monitor the diffusion range of liquid injection, based on seepage numerical simulation results of liquid injection in theoretical models and high-density ERT. Subsequently, field data collection is conducted at the injection site using high-density ERT, and a deep electrical-geological structural model is inverted, which was used to conduct seepage numerical simulation, while dynamic monitoring of leach liquid also be performed using time-lapse high-density ERT. The diffusion characteristics of liquid injection revealed by the two methods are compared and analyzed. Based on the experimental outcomes,an efficient

methodology is proposed for assessing the diffusion range and seepage behavior of liquid injection, integrating "detailed deep structural investigation & numerical simulation of injection seepage."

2. Numerical simulation

2.1 Constrained parameters of seepage numerical simulation

The permeability coefficient reflects the ability of soil to allow water to pass through, primarily governed by the particle size distribution, mineral composition, and formation process of the soil. According to hydraulic principles, changes in water content lead to corresponding variations in the permeability coefficient, and the relationship between them can be described by specialized functions. When measuring the permeability coefficient of saturated soil, undisturbed soil samples are typically used for laboratory experiments or in-situ tests. In the past, many studies employed simple statistical methods to identify patterns in data for determining the permeability coefficient. However, this approach is limited by experimental conditions and often yields insufficiently accurate results. Nowadays, a more commonly used method involves indirectly estimating the permeability coefficient through the soil-water characteristic curve. For unsaturated soil, obtaining the permeability coefficient experimentally is highly challenging, instead, parameters can be derived using the Fredlund model (Fredlund and Xing 1994; Chen et al. 2017) and the Van Genuchten model (Van Genuchten, 1980; Bi and Chen , 2017), and our study selects the latter model to calculate the saturated permeability coefficient, with its formula provided as follows:

$$k_w = k_s \frac{[1-a\phi^{n-1}(1+a\phi^{-mn})]^2}{(1+a\phi^n)^{\frac{m}{2}}} \quad (1)$$

In the formula:：$k_s$is the saturated permeability coefficient；a，m，nare curve-fitting parameters, m=1-$\frac{1}{n}$。

Bao (2023) conducted an measurement of the basic physical parameters and saturated permeability coefficient of the soil in the study region, and the average values of the soil test results are shown in Table 1.

Table 1 Summary Table of Soil Test Results for rare earth ores (Bao, 2023)

Index / Location	Particle Size Distribution			Basic Physical Parameters					Hydraulic Parameters
	d_{10}/mm	d_{30}/mm	d_{60}/mm	C_c	C_u	d_s	n	ρ_d/(g/cm^3)	K_s/(m/d)
Hilltop	0.038	0.353	1.143	2.8	29.7	2.71	0.44	1.50	2.970
Hillside	0.068	0.434	1.264	2.2	18.5	2.70	0.47	1.43	3.847

The permeability characteristics are governed by various geological factors, such as pore structure, particle size distribution, and initial water content (Niu 2006). In ionic rare earth ore strata, the degree of weathering exerts the most significant influence on permeability. For instance, the permeability coefficients of granite strata with different weathering grades can

vary by orders of magnitude, with lower degrees of weathering corresponding to markedly reduced permeability (Zhang et al. 2022). Accurate geological stratification, which relies on detailed and precise exploration data, is essential for obtaining reliable numerical simulation results. Based on high-density electrical resistivity tomography (ERT), this study simplifies the seepage numerical simulation model for liquid injection into three layers: the topsoil layer, the weathered layer, and the bedrock layer.

The material parameters required for seepage numerical calculation mainly include the soil-water characteristic curve, permeability coefficients, and saturated permeability coefficient of each layer. Based on the particle size distribution results of the completely weathered layer shown in Table 1, and with reference to similar projects, the 《Rock Mechanics Parameter Manual》, and the 《Engineering Geology Handbook (Fifth Edition)》, the seepage parameters of each stratum were determined, as shown in Table 2.

Table 2 Seepage Parameters of Different Strata (Bao, 2023)

Parameter		Stratum Name		
		Surface Soil Layer	Weathered Layer	Bedrock
Permeability Coefficient k_s/(m/d)		0.62	1.72	0.17
Residual Water Content θ_w		0.095	0.046	0.041
Saturated Water Content θ_r		0.40	0.46	0.41
Van Genuchten (VG) Model	a/kPa	5.26	1.33	0.81
	n_v	1.31	1.89	2.28
	m	0.24	0.47	0.56

2.2 The identification capability of ERT for seepage range

2.2.1 Seepage numerical simulation in uniform stratum

PLAXIS 2D, developed by the Dutch company PLAXIS B.V., is a high-performance general-purpose geotechnical finite element analysis software known for its powerful computational capabilities, broad applicability, stable operational performance, and reliable result output. Additionally, the software is equipped with robust post-processing functions, further enhancing its practical value. Therefore, this study employs PLAXIS 2D to conduct numerical simulations of single-hole fluid injection in uniform stratum and analyze its seepage characteristics.

The hydrological model has a depth of 10 m and a radial extent of 10 m, discretized into 832 grid cells. The initial groundwater level is set at the bottom of the model. Since only seepage processes are simulated, the key material parameters required include the soil-water characteristic curve, the permeability coefficient function (as a function of saturation), and the saturated permeability coefficient. These parameters are determined based on particle size distribution data and soil classification (loamy sand is selected), with detailed information provided in Fig. 1. The steady-state seepage results under an average annual rainfall rate of 3 mm/d are used as the initial condition for the simulation, corresponding to a soil saturation of

approximately 47%, as shown in Fig. 2a.

Fig. 2 presents the saturation distribution cloud images of loamy sand at different time points. After the liquor is injected into the ore body, it permeates along both horizontal and vertical dimensions under the combined influence of matrix suction and gravity, gradually transforming the originally dry soil from an unsaturated state to a saturated state. As the injection continues, the shape of the wetted body evolves from an initial semicircle to a semi-ellipse. Meanwhile, the overall diffusion rate undergoes a rapid decline phase until reaching a relatively stable level. Additionally, the infiltration process of the liquor exhibits nearly uniform diffusion within the unsaturated medium.

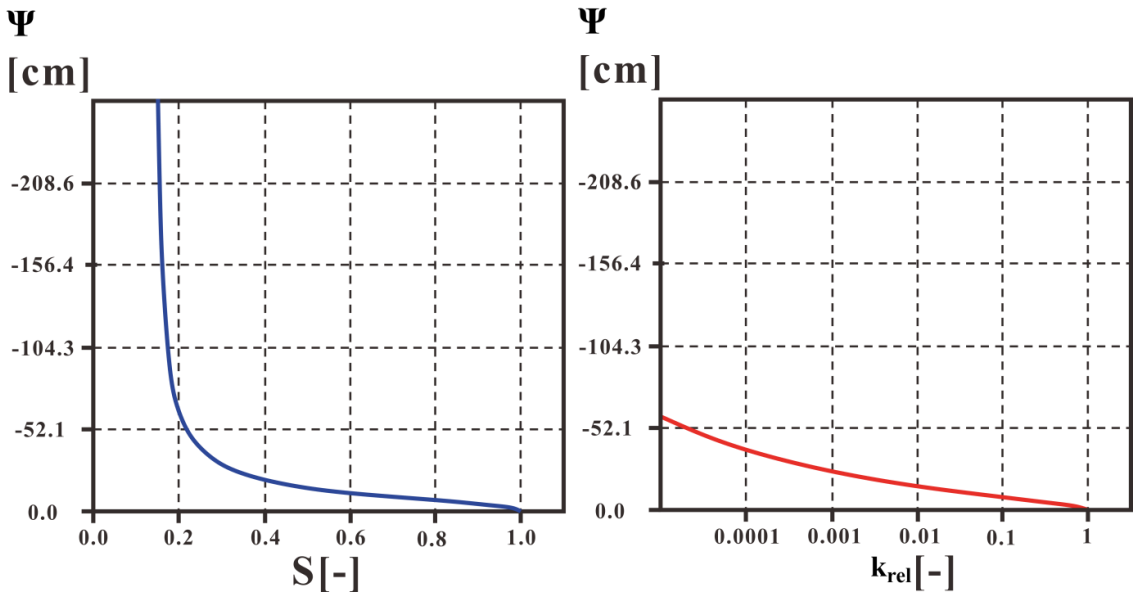


Fig. 1 Soil-Water Characteristic Curve and Hydraulic Conductivity Curve for Loamy Sand

2.2.2 Resistivity models for high-density ERT simulation

The detection resolution and depth of the high-density ERT method is closely related to the acquisition system used (Zheng et al. 2015). To evaluate the effectiveness of ERT in exploring the diffusion range of leach liquor under different acquisition systems, this section constructs establishes resistivity structure models (shown in Fig. 3) for three time points (T1=1 day, T2=2 days, T3=3 days) based on the diffusion ranges of the leach liquor revealed in Fig. 2, within which the diffusion radii of the leach liquor are R1=0.5 m (T1), R2=1.5 m (T2), and R3=3 m (T3). The background resistivity of the model is set to 1000 Ω·m (weathered granite layer), while the resistivities of the core affected area and the peripheral area of the liquor injection are set to 50 Ω·m and 100 Ω·m, respectively. Subsequently, numerical simulations and inversion calculations were conducted using Res2dmod and Res2dinv software. The calculation results for the Wenner, Wenner-Schlumberger, and dipole-dipole acquisition systems are shown in Fig. 4, which serve to assess the response capability of the high-density ERT in imaging the seepage process.

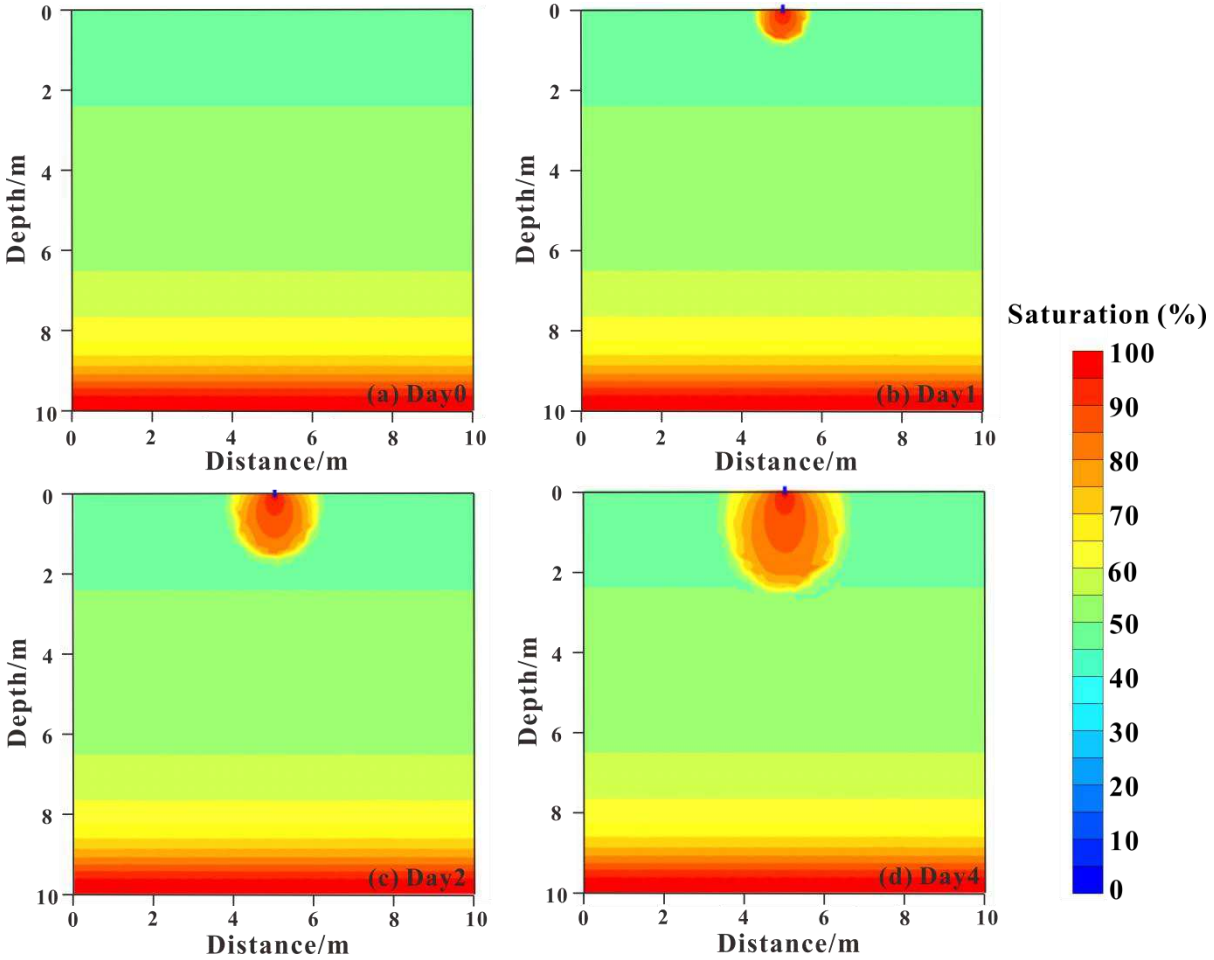


Fig. 2 Contour of Soil Saturation Distribution at Different Times

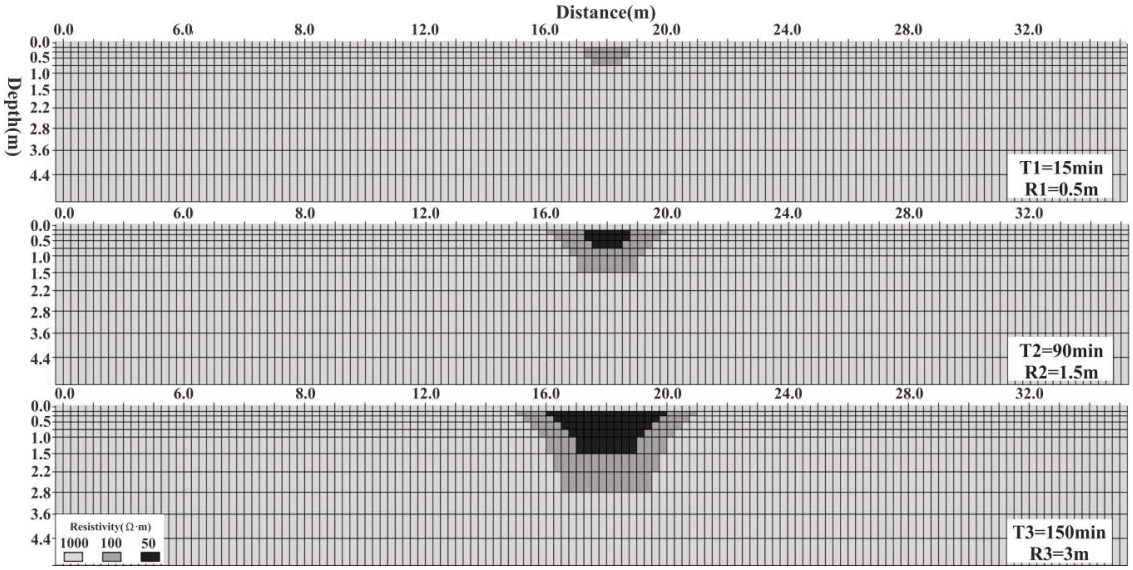


Fig. 3 Numerical Simulation Geoelectrical Model

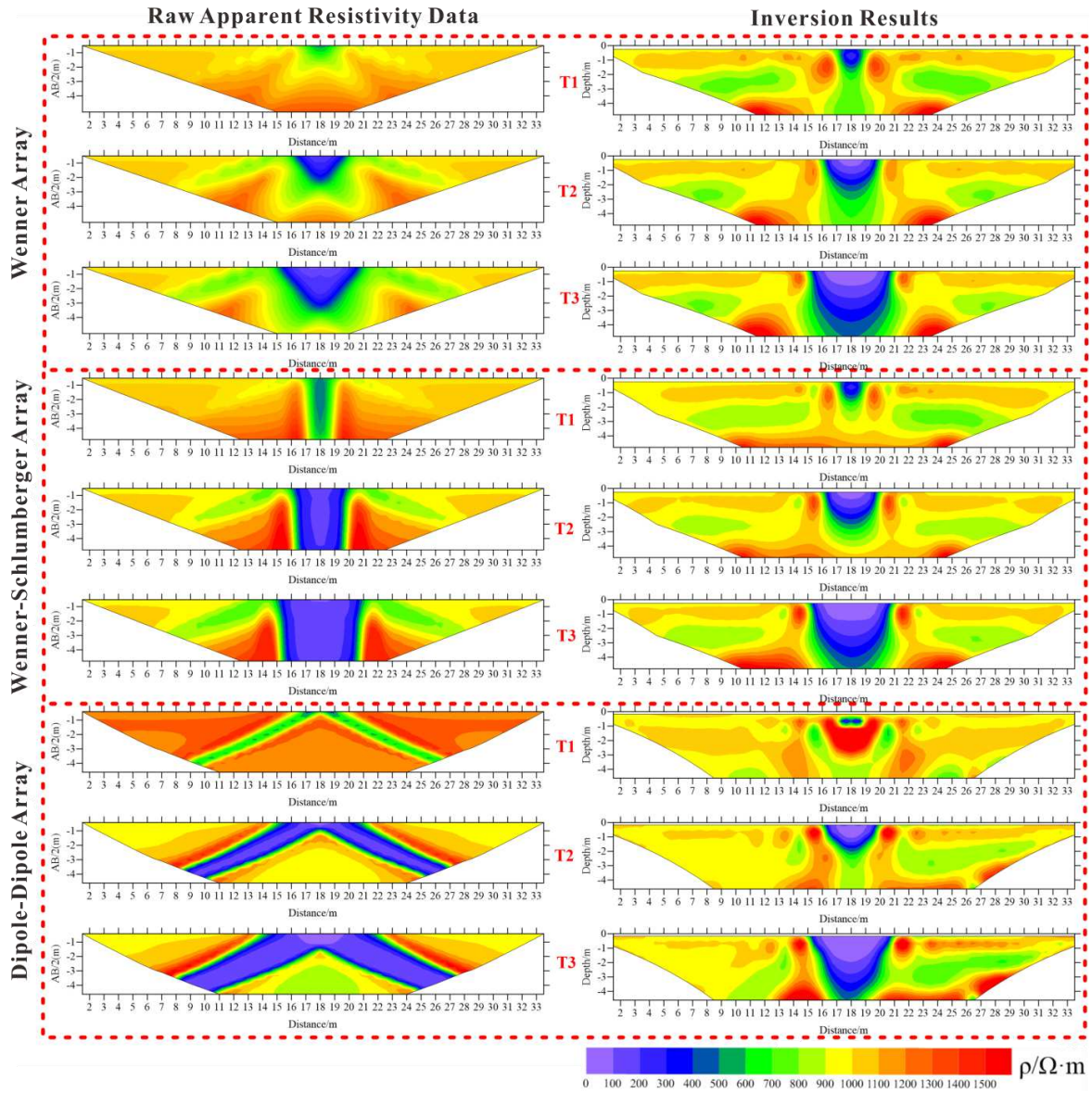


Fig. 4 Numerical Simulation Results of Electrical Resistivity Tomography with Different Arrays at Various Injection Times

2.2.3 High-density ERT simulation for seepage range

As shown in Fig. 4, there are certain differences in the forward and inversion results of high-density ERT for different acquisition systems at various liquid injection times. From the perspective of forward modeling results,the original apparent resistivity cross-sections vary significantly due to the distinct electrode arrays used in the three systems; nevertheless, all systems roughly identify the horizontal position of the anomalous zones. Among them, the Wenner system's original apparent resistivity cross-sections at times T1, T2, and T3 relatively intuitively depict the extent and variation characteristics of the anomaly zones. In the early stage of liquor diffusion (time T1), the inversion results of the three arrays show some discrepancies, however, as the diffusion range of the liquor expands (times T2 and T3), the inversion results clearly reflect the horizontal and vertical diffusion of liquor injection. Overall, the Wenner and Wenner-Schlumberger systems outperform the dipole-dipole system. They not only capture the vertical variations in subsurface resistivity but also reflect horizontal characteristics to some extent, yielding inversion results that are closer to the actual situation

and thus more effective. As shown in Fig. 4, although the dipole-dipole system is recognized for its high horizontal resolution and is well-suited for detecting shallow geological structures or interfaces (Zheng et al. 2015), its performance in delineating the diffusion range of liquid injection is inferior to that of the Wenner system.

All three acquisition systems of the High-density ERT can reflect the diffusion of the leach liquor in the inversion results. However, compared to the dipole-dipole system, both the Wenner and Wenner-Schlumberger systems provide better constraints on the diffusion boundary of the solution. Moreover, the Wenner system allows for an intuitive visualization of changes in anomaly zones directly from the apparent resistivity. Therefore, the Wenner system was adopted for subsequent numerical simulations and field data acquisition.

2.3 Influence of geological structures on seepage

Ionic rare earth ores are primarily distributed within the weathered layers of granite, where the diffusion of leach liquor is mainly controlled by the spatial morphology of the bedrock (intact granite) and the fractures within it. In-situ leaching is a complex seepage process involving both saturated and unsaturated states, and the seepage phenomenon of the liquor is constrained by multiple factors. To analyze the influence of subsurface structures on the flow direction and diffusion range of the injected liquor, this study establishes models for different subsurface structures under the conditions of a single-hole injection rate of 5.0 m^3/d, an initial groundwater level of -50 m, and an injection duration of 40 days, aiming to examine the patterns of liquor diffusion during the leach process.

（1）Seepage simulation on model with undulating bedrock top surface

Fig. 5 shows the geological structure and grid division results. The lithology primarily consists of weathered granite layers and intact granite bedrock. Through seepage numerical simulation, the impact of varying burial depths of the bedrock top surface on the diffusion range of liquid injection is analyzed.

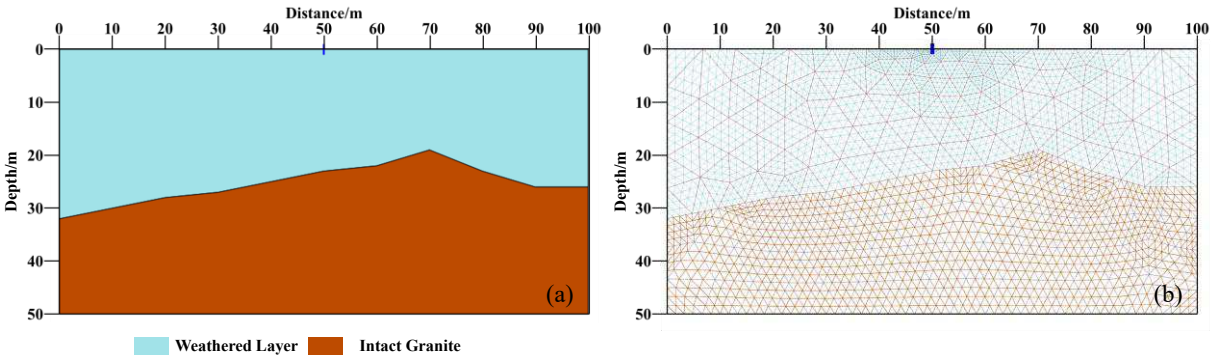


Fig. 5 Bedrock Surface Undulation Model: (a) Model Geometry, (b) Mesh Generation

Fig. 6 shows the saturation distribution maps of the model with undulating bedrock top surface at different times. In the weathered layer, the injected liquid diffuses uniformly without obvious preferential flow characteristics. As time progresses, when the saturated zone expands into the intact granite bedrock with relatively lower permeability coefficient, the vertical extension of the saturated zone is hindered, developing a characteristic of lateral preferential permeability. Meanwhile, due to variations in the burial depth of the bedrock surface, the

diffusion of the liquid injection exhibits significant anisotropy, demonstrating a pattern of "lateral preferential seepage with hindered vertical seepage." By Day 20, as the burial depth of the bedrock surface is greater on the left side, the diffusion of the injected liquid is more pronounced on this side. By Day 40, the saturated zone on the left extends approximately 40 meters, while the saturated zone on the right expands only about 25 meters.

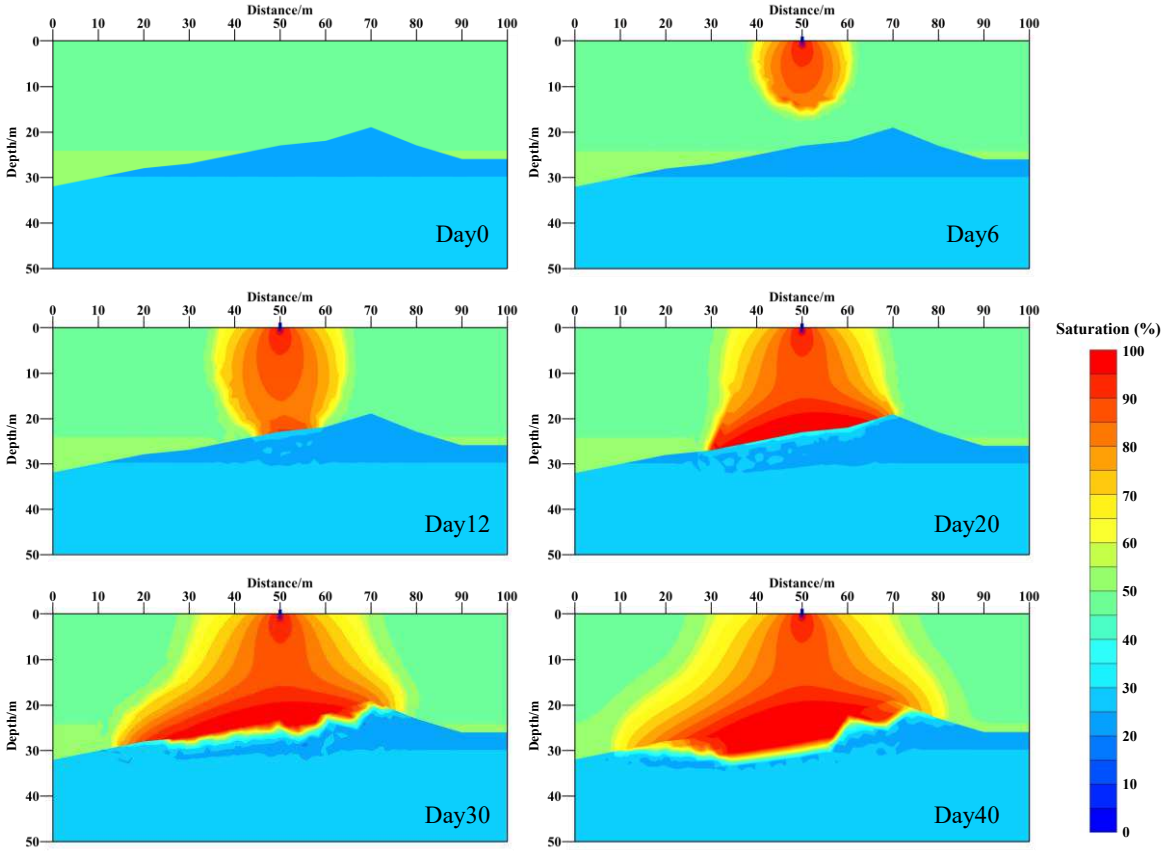


Fig. 6 Contour of Saturation Distribution for the Bedrock Undulation Model at Different Times

（2）Seepage simulation on model with tilted fault fracture zone

Fig. 7 shows the geological structure with tilted fault fracture zone and grid division results. The lithology primarily consists of weathered granite layers and intact granite bedrock. Through seepage numerical simulation, the impact of tilted fault fracture zone on the diffusion range of liquid injection is analyzed.

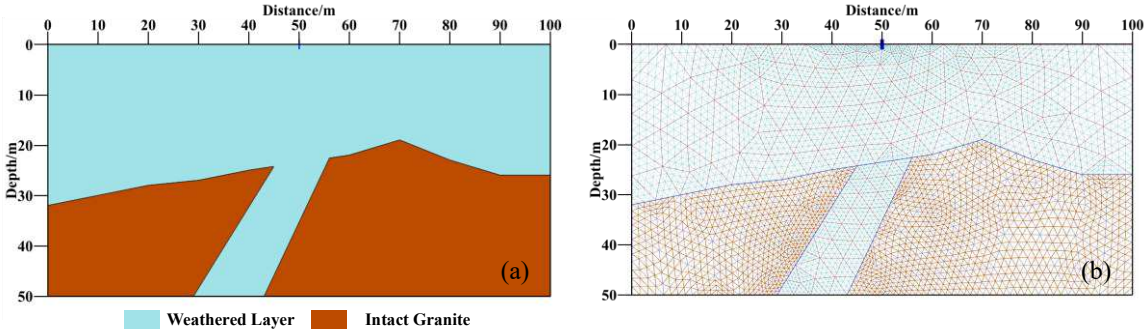


Fig. 7 Inclined Fracture Zone Model: (a) Model Geometry, (b) Mesh Generation

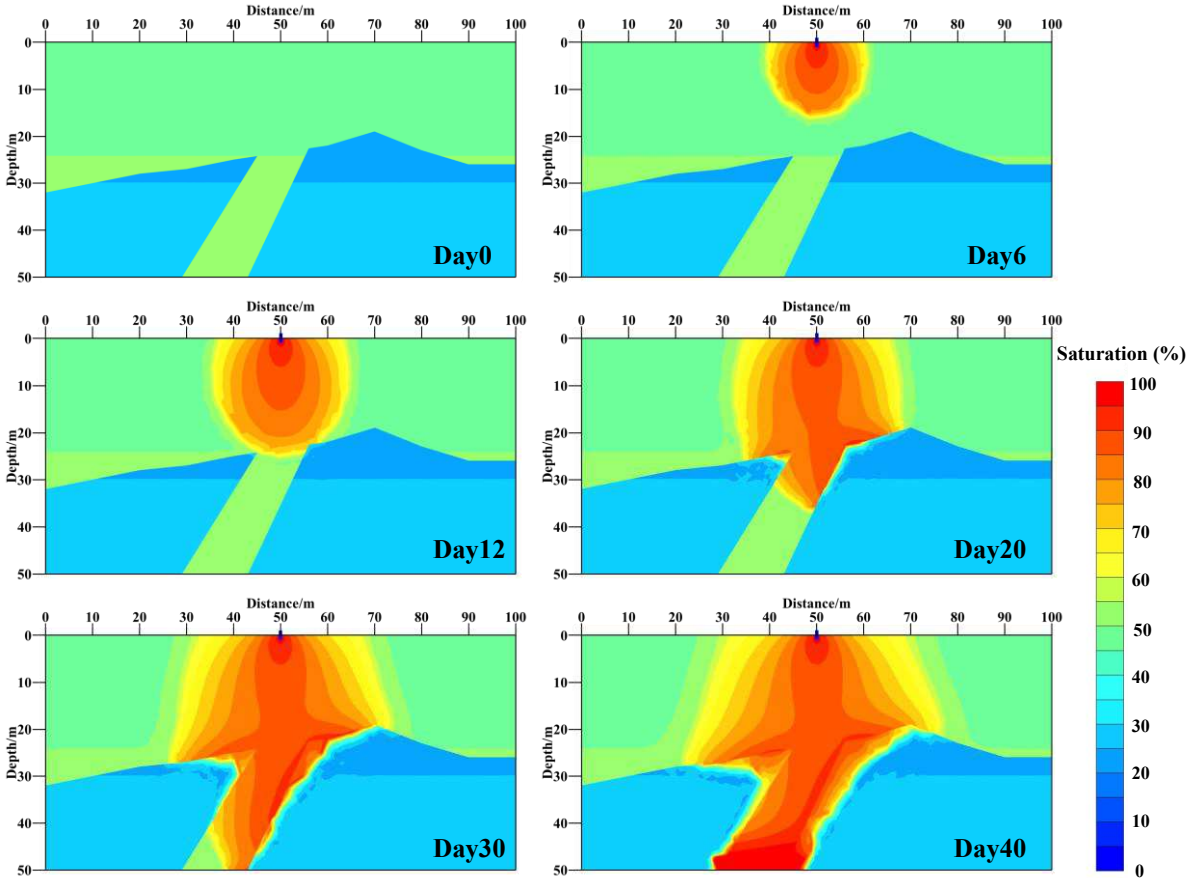


Fig. 8 Contour of Saturation Distribution for the Inclined Fracture Zone Model at Different Times

Fig. 8 shows the saturation distribution maps at different times. In the weathered layer, the injected liquid diffuses uniformly without obvious preferential flow characteristics. As time progresses, when the saturated zone expands into the granite bedrock, due to the presence of fault fracture zones with high permeability coefficients, the injected fluid predominantly permeates into the fractured zones of the bedrock and shows significant vertical extension. Particularly between Day 30 and Day 40, the lateral expansion of the saturated area weakened, and the fluid flow occurred only along the dip direction within the fracture zones.

（3）Seepage simulation on granite boulder model

Fig. 7 shows the geological structure with isolated rock and grid division results. The lithology primarily consists of weathered granite layer, intact granite bedrock, and granite boulder. Through seepage numerical simulation, the impact of granite boulder on the diffusion range of liquid injection is analyzed.

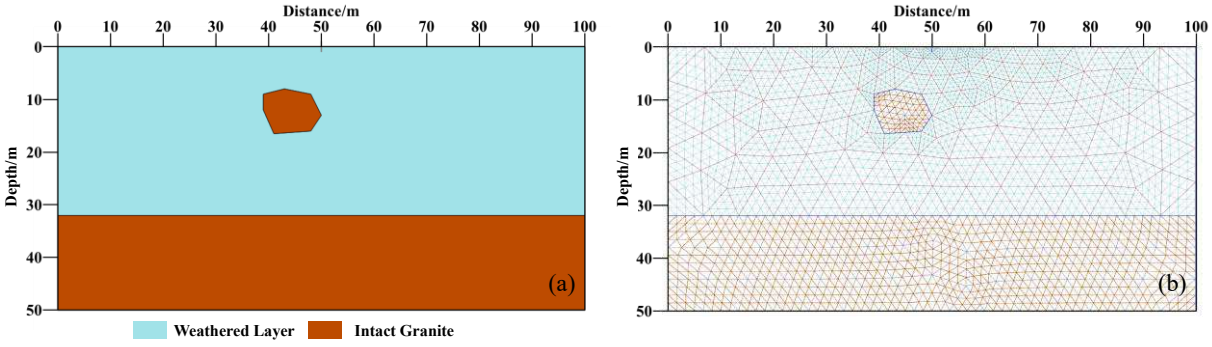


Fig. 9　Small-Scale Boulder Model: (a) Model Geometry, (b) Mesh Generation

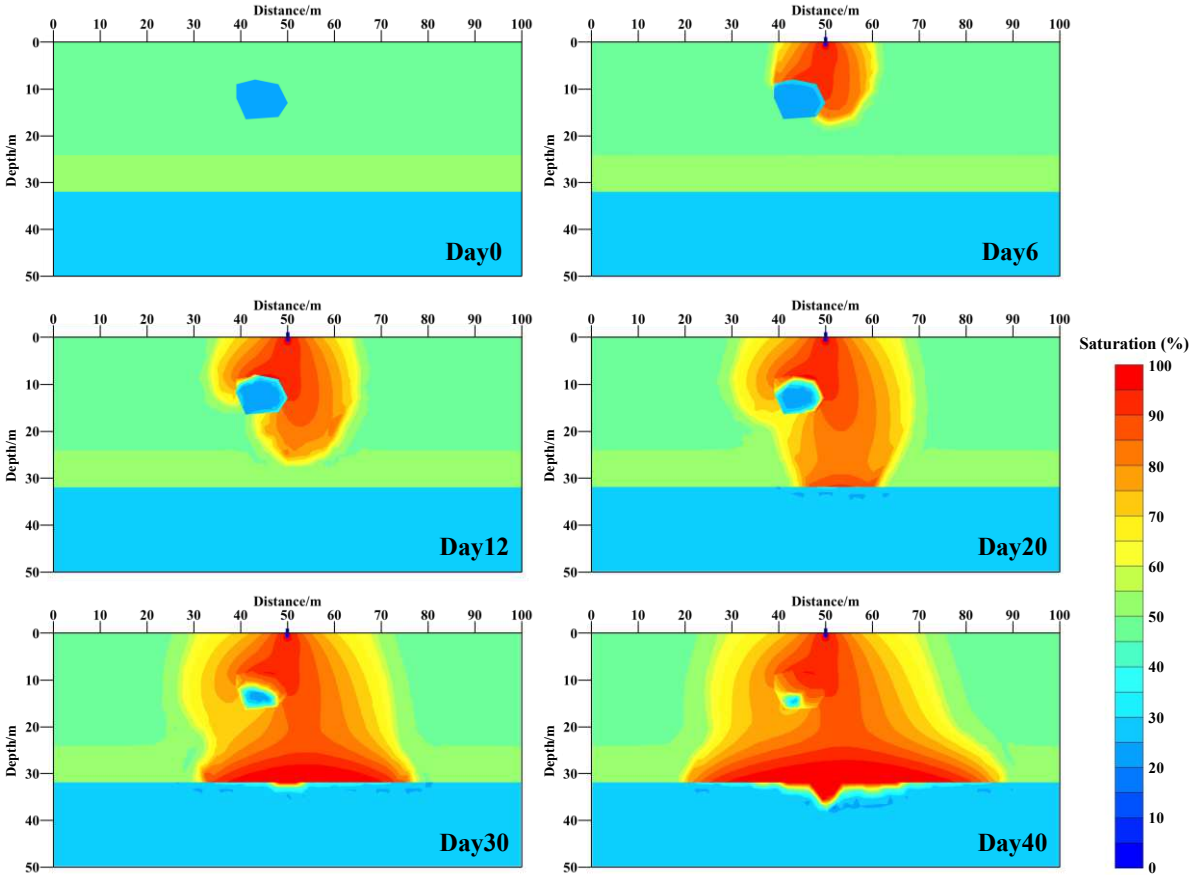


Fig. 10　Contour of Saturation Distribution for the Boulder Model at Different Times

Fig. 9 shows the distribution of saturation in the boulder model at different times. In the weathered layer, liquid injection is influenced by the granite boulders, resulting in anisotropic diffusion characteristics. Due to the poor permeability of the granite boulder on the left side of the injection hole, vertical seepage on the left is affected, and no significant vertical diffusion is observed in the saturated zone. When the saturated zone reaches the granite bedrock, the vertical seepage velocity slows down, exhibiting characteristics of preferential horizontal flow. Influenced by the shallow granite boulders, the changes in the saturated zone are more pronounced on the right side, particularly on Day 30 and Day 40, where the saturated zone expands further to the right.

（4）Seepage simulation on complex geological model

Fig. 11 illustrates the structure of the complex geological model and its mesh division. The model incorporates structural information such as faults, boulders, and undulating bedrock surfaces, with lithology primarily consisting of weathered granite layers and intact granite. Seepage simulation is employed to analyze the comprehensive impact of complex geological structures on the diffusion range of fluid injection.

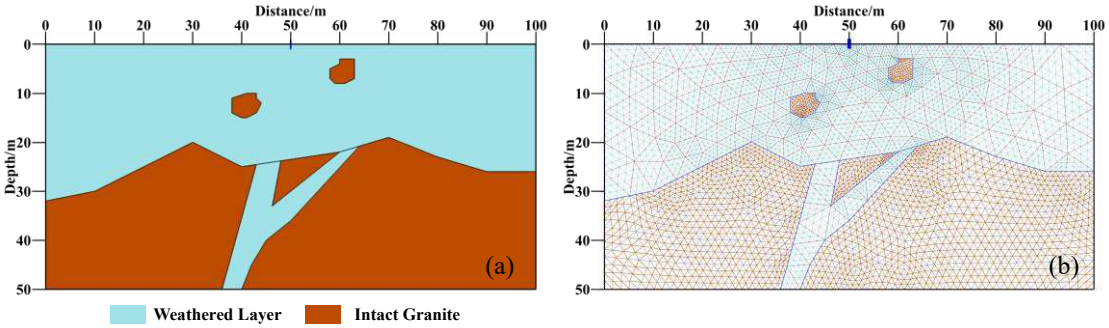


Fig. 11. Complex Geological Model: (a) Model Geometry, (b) Mesh Generation

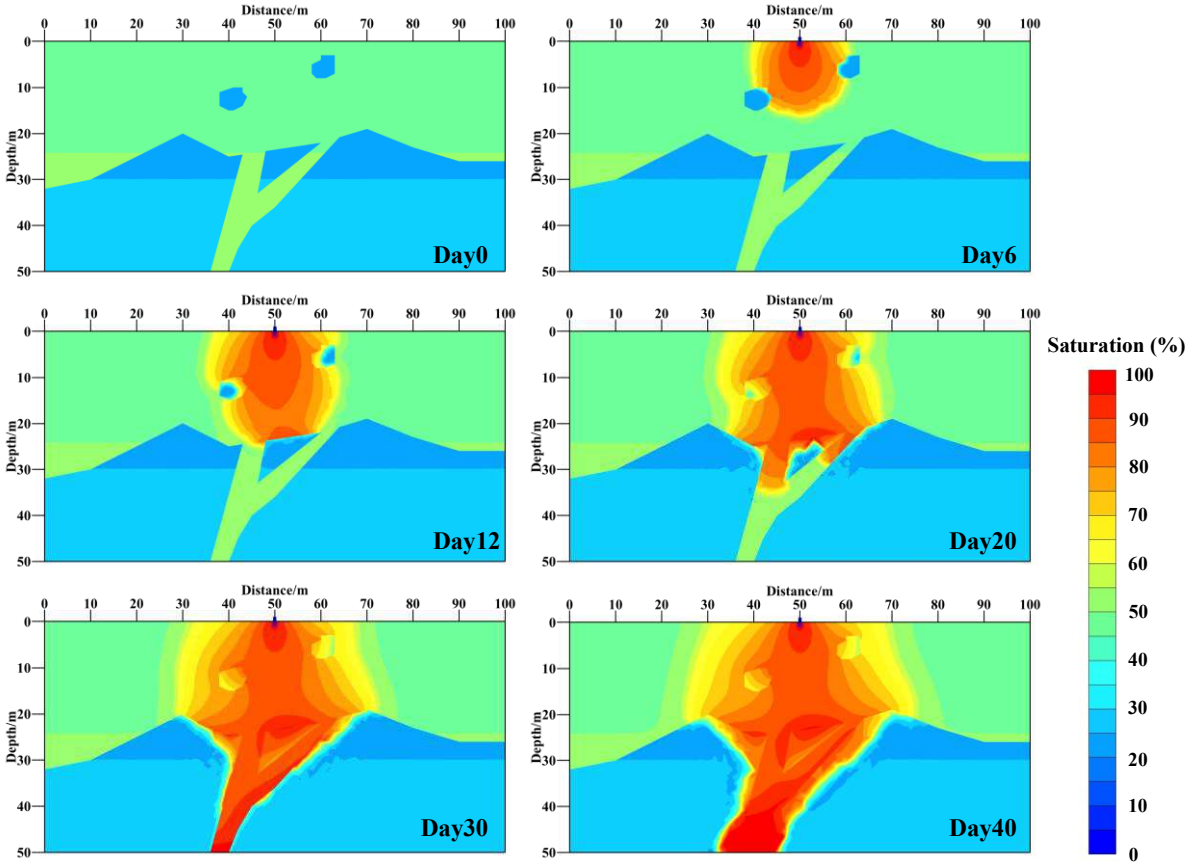


Fig. 12 Contour of Saturation Distribution for the Complex Geological Model at Different Times

Fig. 11 shows the saturation distribution maps of the complex geological model at different times. It can be observed that due to the low permeability of the intact granite boulders on the left and right sides, the seepage velocity is affected. Shallowly buried boulders have a greater impact on lateral diffusion, while deeply buried boulders influence vertical diffusion more significantly. When the saturation zone reaches the intact granite bedrock, the vertical seepage velocity decreases. However, due to the presence of two fracture zones in the granite bedrock, the injection exhibits a distinct seepage characteristic aligned with the dip direction of the fracture zones.

From the above seepage simulation results, it can be seen that boulders, fracture zones, and the undulation of the bedrock surface all influence the seepage range of the injection fluid. Among these, the varying distances between boulders and the injection boreholes result in

different characteristics of seepage influence. The fracture zones developed in bedrock have the most significant impact on the seepage, primarily manifested as the injected fluid escaping along the fracture zone. Therefore, for ionic rare earth ores, detailed detection of the underground structure in the mining area can provide important references for the precise placement of injection boreholes during the in-situ leaching process.

3. Comparison of time-lapse monitoring and seepage simulation

3.1 Detection of deep structures in the monitoring area

A high-density ERT profile was deployed at a rare earth ore in Fujian Province of China (Fig. 13), with a total length of 270 m and an station spacing of 2.5 m. D1 represents a previously injected area, while D2 is a non-injected area. This high-density ERT profile spans both D1 and D2, allowing for an effective comparison of the deep electrical structures before and after liquid injection.

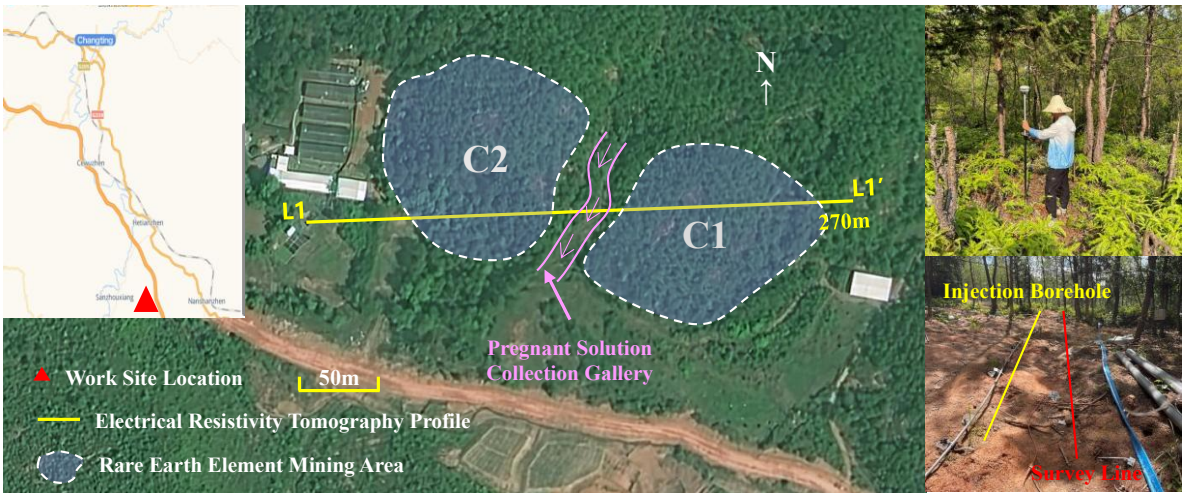


Fig. 13 Study Area Topography and Survey Line Layout

The 2D inversion was conducted using the Res2dinv software, with an initial damping coefficient of 0.16 and a vertical/horizontal smoothing ratio set to 1.5. The resistivity range for the inversion was constrained between 1 and 5000 Ω·m. During the inversion process, parameters were dynamically adjusted based on the intermediate results, ultimately achieving a root mean square error of less than 6%. The inversion results are shown in Fig. 12.

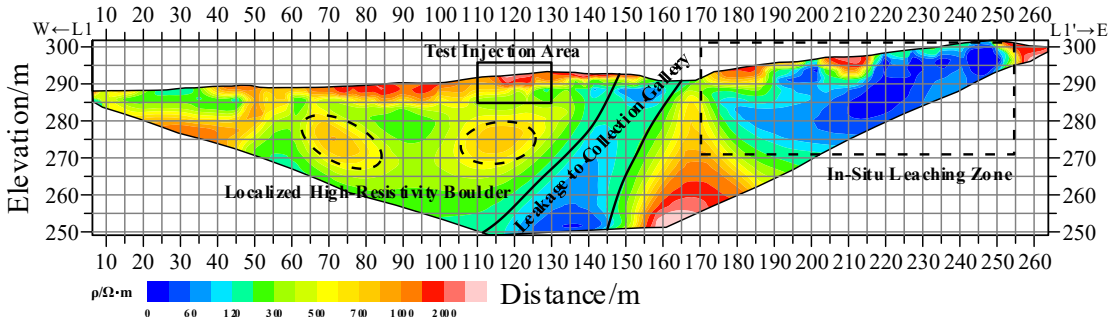


Fig. 14 Inverted Resistivity Profile from Electrical Resistivity Tomography Survey Prior to Fluid Injection

As shown in Fig. 13, the section from 10-120m in lateral distance exhibits a medium resistivity characteristic, with localized high resistivity inferred to be granite boulders. The

section from 120-140m in lateral distance shows a low-resistivity band anomaly C1 dipping westward, with values ranging from 10-100 Ω·m. Since the recovery tunnel for the C3 ore body leachate is located in this section, the anomaly C1 is interpreted as relatively low resistivity resulting from longitudinal leakage of the injected liquid. The section from 150-190m in lateral distance displays relatively high resistivity, with values exceeding 100 Ω·m, corresponding to semi-weathered and intact granite formations. The section from 190-260 m in lateral distance exhibits relatively low resistivity anomaly C2, with resistivity values below 50 Ω·m, which is a comprehensive response of the formation after liquid injection. The significant difference in formation resistivity before and after liquid injection demonstrates the theoretical feasibility of monitoring changes in subsurface resistivity during liquid injection and analyzing liquid migration patterns based on electrical structure.

3.2 Time-lapse ERT monitoring

This study selects the lateral mileage range of 110-130m along the high-density ERT profile as the time-lapse monitoring test area for liquid injection. The area is characterized by vertically developed low-resistivity weathered layers overlying high-resistivity granite, which allows for an effective investigation of the diffusion of liquid injection through time-lapse resistivity variations, while also enabling an evaluation of the influence of intact granite on the seepage.

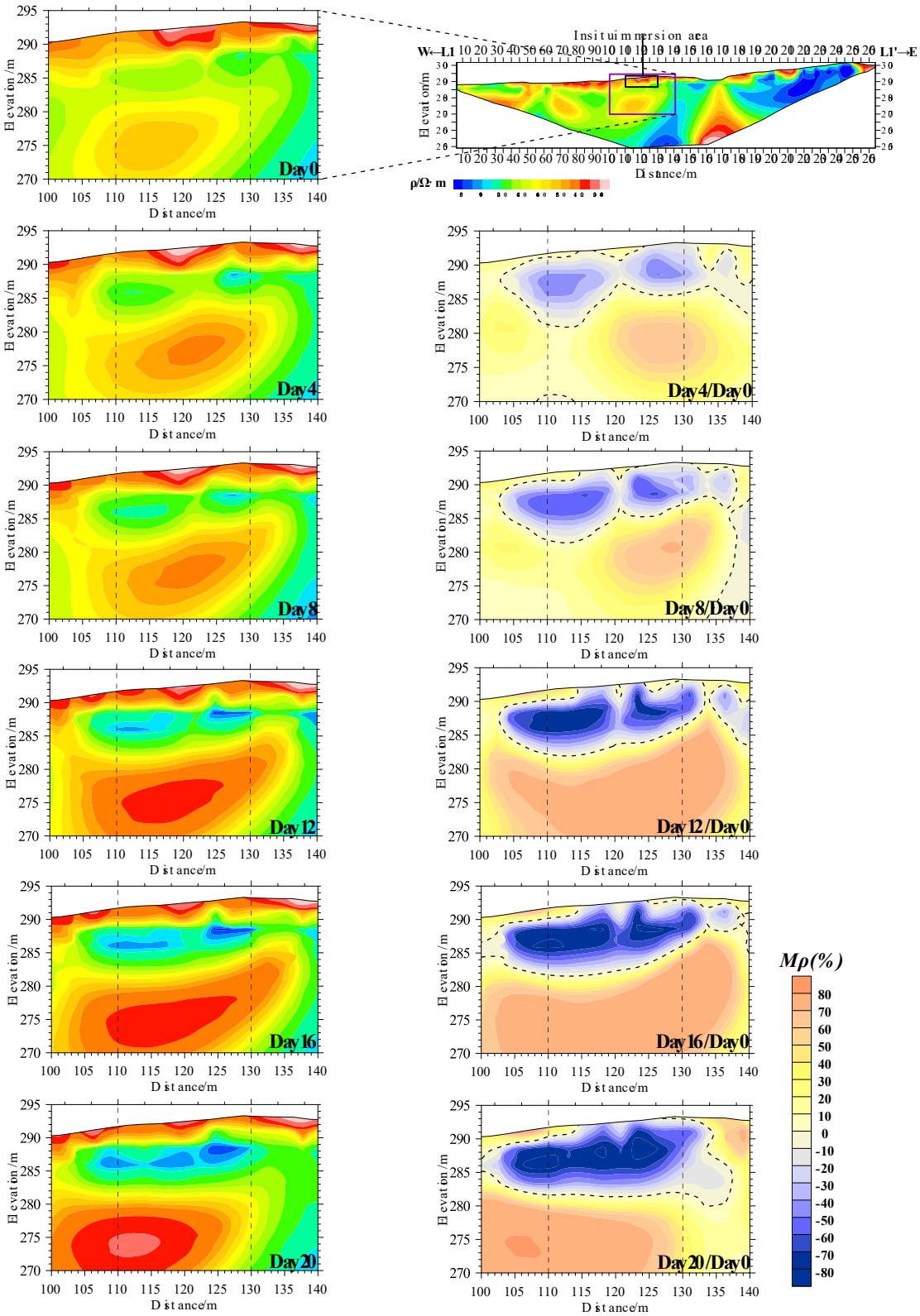


Fig. 15 Inverted Resistivity Profiles and Resistivity Change Rate ($M\rho$) Profiles from Electrical Resistivity Tomography at Different Times During Injection

The high-density ERT data acquisition was completed three hours after daily fluid injection. The time-lapse monitoring spanned 20 days, and this study selects 11 sets of data for analysis. The inversion resistivity during the injection period and its change rate(Mρ) maps are

shown in Fig. 15. As injection time progresses, the subsurface resistivity in the injection area changes significantly, with most resistivity values dropping from above 1000 Ω· m to below 100 Ω· m, reaching as low as 20 Ω· m. Vertically, due to the low permeability of granite, the resistivity reduction zone only reaches a depth of 10 m, and injected fluid primarily exhibits lateral migration at this depth. Horizontally, the change in resistivity is relatively pronounced, extending from the central injection area toward both east and west sides, with a farther migration distance of about 5 m to the west (left) side. On the east (right) side, the intact granite roof is shallower, acting as a barrier, resulting in a smaller diffusion range of the injected fluid. Overall, the fluid migration is characterized by "rapid lateral diffusion in shallow layers and restricted vertical migration in deeper layers." In addition, as shown in Fig. 15, the maps of the resistivity change rate Mρ show significant anomalies at different times. The negative value zone of the resistivity change rate Mρ exhibits a clear expansion over time, with its extent largely consistent with the distribution range of low resistivity. However, the Mρ provides better precision in boundary delineation compared to the resistivity inversion results.

3.3 Seepage simulation in the monitoring area

The numerical simulation was conducted within the lateral range of 110-130 m along the high-density ERT profile. The initial model of the liquid injection area was established using PLAXIS 2D software, as shown in Fig. 14. The lithology primarily consists of topsoil, weathered layer, and intact granite boulders, with permeability decreasing in that order. Two sets of injection holes were designed, with a spacing of 2 m between holes. The numerical simulation results are presented in Figure 17.

At the beginning of fluid injection, the seepage is relatively uniform, with the high-saturation distribution zones around the two sets of injection holes exhibiting an elliptical shape. When encountering intact granite with low permeability, preferential lateral seepage pathways develop, leading to non-uniform flow. As injection time increases, the saturation within the injection zone gradually rises. Vertically, due to the barrier effect of the intact granite, the extension of the high-saturation zone is not significant. Laterally, however, the changes in the high-saturation zone are more pronounced, extending from the central injection area toward the east and west sides. Influenced by the undulating top surface of the intact granite, the saturation extends farther toward the west (left) side, reaching a distance of 10 m in the saturation map at Day 20, which is consistent with the anomalous response pattern of the resistivity change rate M ρ mentioned above.

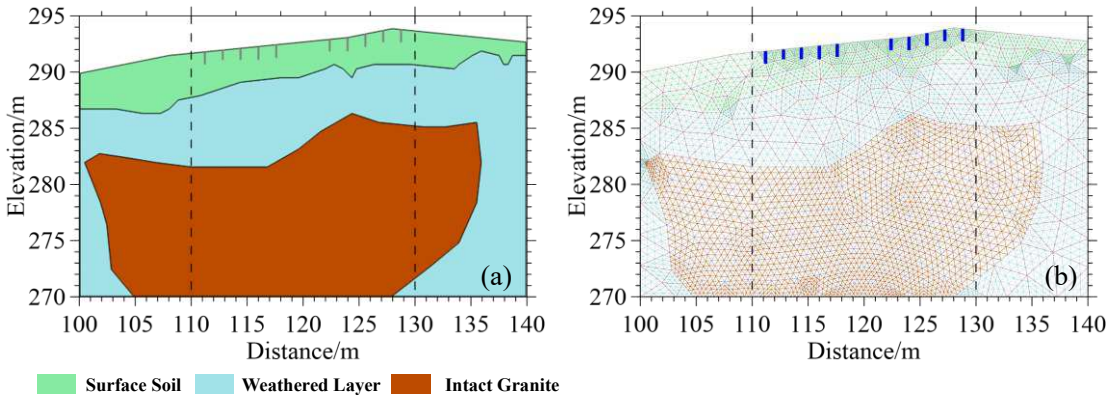


Fig. 16 Subsurface Structure Model of the Injection Area: (a) Model Geometry, (b) Mesh Generation

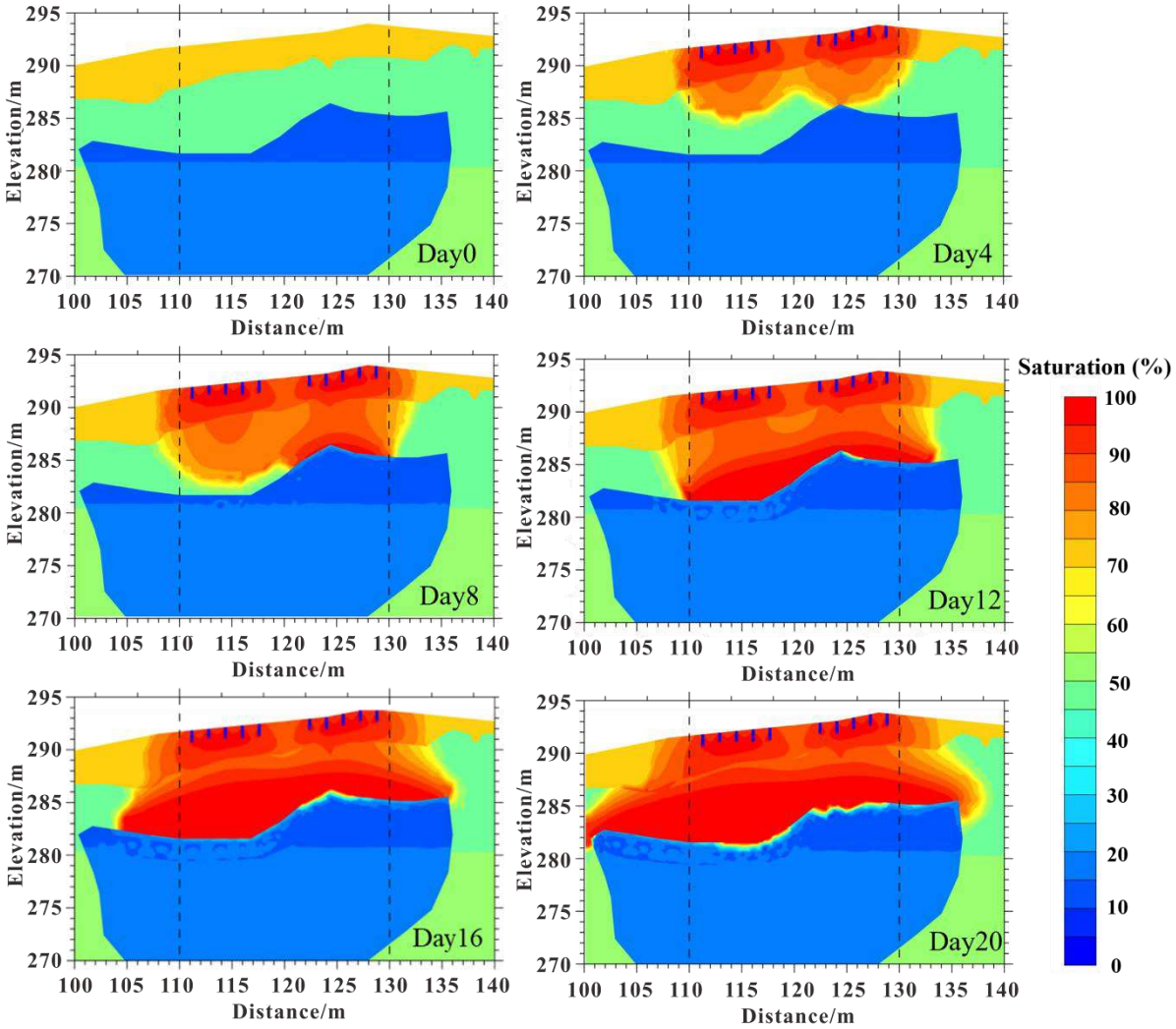


Fig. 16 Contour of Saturation Distribution at Different Times for the Model Cross-Section

The simulation results of liquid injection indicate that the distribution of high saturation zones in the injection area is largely consistent with the negative value zones in the resistivity change rate (M ρ) map, which accurately reflects the diffusion pattern of the injected liquid and demonstrates the influence of the undulating granite top surface on the seepage behavior. Therefore, employing geophysical methods to detect the deep fine structure of ion-adsorption rare earth ores and conducting seepage numerical simulation analysis based on this refined

structure can effectively assess the seepage characteristics of liquid injection. This provides a scientific reference for the distribution of injection holes and the layout of recovery galleries during in-situ leaching mining of ion-adsorption rare earth ores.

4. Conclusion

This study employs time-lapse ERT and numerical simulation methods to compare and analyze the effectiveness of numerical simulation results and actual monitoring results in identifying the diffusion range of liquid injection in ion-adsorption rare earth ore. The main conclusions are as follows:

(1) The results from both seepage simulation and high-density electrical resistivity tomography (ERT) simulation show that the resistivity in the diffusion zone of the injected liquid decreases significantly and corresponds well with the seepage range of the leachate. The diffusion behavior of the leach liquid is not only influenced by the permeability coefficient of the medium, but is also strongly controlled by the spatial distribution characteristics of structural parameters such as fractures, isolated rock bodies, and bedrock surface undulations. Variations in these parameters result in significant anisotropy in the diffusion range of the leach liquid.

(2) When granite boulders develop within the weathering layer, the leach liquid diffuses at a higher rate on the side where the burial depth of the top surface of the boulder is greater. Compared to the undulating morphology of the bedrock granite, bedrock fractures exert a stronger control over the diffusion characteristics of the injected liquid. The resistivity change rate (M ρ) reflects the diffusion of the liquid injection and outperforms resistivity inversion results in terms of boundary delineation precision. Additionally, it can identify the influence of the undulating granite top surface on the diffusion range of the leach liquid.

(3) Based on a comparative analysis of time-lapse high-density ERT monitoring and seepage numerical simulations in actual geological structures, an efficient solution for analyzing liquid injection diffusion characteristics has been proposed. This approach, which combines "detailed deep structure investigation & seepage numerical simulation of liquid injection" can overcome the drawbacks of full-domain time-lapse geophysical monitoring, such as difficulties in implementation, high costs, and poor timeliness.

Acknowledgments

We thank the Longyan Rare Earth Development Co., Ltd., China, for providing the help in data acquisition. This work is supported by the Deep Earth Probe and Mineral Resources Exploration-National Science and Technology Major Project (2024ZD1001003). Several figures are created with Generic Mapping Tools.

References

Bao JP (2023) Modification of calculation formula of single ring permeability test and its application to seepage simulation of in situ leaching. Jiangxi University of Science and Technology, China. https://doi.org/10.27176/d.cnki.gnfyc.2023.000969

Bi J, Chen WW(2017) Influence of forms of parameter m and largest matric suction point on the parameters of Van Genuchten model. Rock and Soil Mechanics 38(12): 3604-3612. https://doi.org/10.16285/j.rsm.2017.12.027

Chen BF, Yang B, Zhang XW, Zou ZQ, Xiao WG, Mo HH, Wu YG, Deng YC, Qian YT, Huang B (2023) 3D Fine Exploration Technology in Productive Exploration of Ionic Type Rare Earth Mine—An Example from Ganzhou. Chinese Rare Earths, 44(6): 38-50. https://doi.org/10.16533/J.CNKI.15-1099/TF.202306005

Chen DG (2019) Experimental Study on Ammonium-free Leaching Reagent for Ion-type Rare Earth Ore. Mining and Metallurgical Engineering 39(2): 89-92. https://doi.org/10.3969/j.issn.0253-6099.2019.02.022

Chen WW, Bi J, Shen YX, Li WJ, Lu K, Liu W (2017) Reliability research on fitting particle size distribution curves of relic soils in arid and semi-arid regions by modified Van Genuchten model. Rock and Soil Mechanics 38(2): 341-348. https://doi.org/10.16285/j.rsm.2017.02.005

Fredlund DG, Xing A (1994) Equations for the soil-water characteristic curve. Canadian Geotechnical Journal 31(4): 521-532. https://doi.org/10.1139/t94-061

Kang SC, Wang GF, Ling BW, Xu YJ, Liang XL, Zhu JX, He HP (2025) Research Progress on Mining Mechanism of Ion-Adsorption Type Rare Earth Ore. Journal of the Chinese Society of Rare Earths 43(02): 268-283. https://doi.org/10.11785/S1000-4343.20250204

Li CT, Min G, Liu K, Shu RB, Si FH, Sun YQ (2024) Three-dimensional numerical simulation and case analysis of deep leakage channel based on multi-electrode resistivity method. Computing Techniques for Geophysical and Geochemical Exploration 46(6): 725-734. https://doi.org/l0.3969/j.issn.l00l-l749.2024.06.ll

Luo F, Yan JY, Liang J, Zhang S, Wu DH, Rao GW, Hu WQ, Fu GM (2024) Application Status and Prospect of Geophysical Technology in Rare-Earth Resources Field. Journal of the Chinese Society of Rare Earths 42(6): 1088-1101. https://doi.org/10.11785/S1000-4343.20240605

Min G, Shu R.B, Liu K, Cheng R, Chen S, Yuan HL (2022) Exploration test of 3D deep structure and floor fracture zone in ion-adsorption type rare earth (ITRE) ore area. The Chinese Journal of Nonferrous Metals 32(6): 1833-1843. https://doi.org/10.11817/j.ysxb.1004.0609.2022-40165

Netto LG, Orlando PD, Serafim R, De Oliveira MP, Pereira JPS, Heleno AF, Spinelli TM, Arbieto CC (2025) Monitoring water percolation in a laboratory compacted soil dam using time-lapse electrical resistivity tomography. Scientific Reports 15: 14356. https://doi.org/10.1038/s41598-025-99325-w

Niu JZ, Yu XX, Zhang ZQ (2006) The present and future research on preferential flow. Acta Ecologica Sinica 26(1): 231-243. https://doi.org/10.3321/j.issn:1000-0933.2006.01.030

Tang LB, Wang P, Chen W, Han YW, Jin YN, Peng ZL, Chen WQ (2024) China's rare earths trade flow analysis: Trade patterns and strategic insights. Bulletin of Chinese Academy of Sciences 39(12): 2074-2085. https://doi.org/10.16418/j.issn.1000-3045.20240912004

Van Genuchten MTh (1980) A closed-form equation for predicting the hydraulic conductivity of unsaturated soils. Soil Science Society of America Journal 44(5): 892-898.
https://doi.org/10.2136/SSSAJ1980.03615995004400050002X

Wang CY, Luo YX, Wang XX, Zhou ZG, Wu QB, Chen M (2025) Technical model of "Source-Flow-Sink" integration for pollution control of residual ammonia nitrogen after in-situ leaching of ion-type rare earth ore. Nonferrous Metals Science and Engineering 16(02): 316-322. https://doi.org/10.13264/j.cnki.ysjskx.2025.02.017

Wang JH, Zhang X, Chen DG, Ma C (2015) Influence of during south ion-absorbed-type rare earth deposit mining on

groundwater and it's monitoring. Science & Technology Review 33(18): 23-27. https://doi.org/10.3981/j.issn.1000-7857.2015.18.003

Wei X, Zhao C, Wang X, Hu LZ, Wang SY, Wang Q, Wang SQ (2024) Thoughts on the sustainable development of rare earth industry in China. Mineral Exploration 15(S2): 732-738. https://doi.org/10.20008/j.kckc.2024s2095

Wen LF, Li YL (2025) Analysis of the causes of excessive leakage in the fractured rock masses of the Ludila hydropower station dam foundation. Bulletin of Engineering Geology and the Environment 84: 191. https://doi.org/10.1007/s10064-025-04212-3

Xie YW, Qi FY, Que XH, Chen BF(2018) The Relevant Problems of Ion-absorption Type REE Deposits Exploration . Chinese Rare Earths 39(6): 122-128. https://doi.org/10.16533/J.CNKI.15-1099/TF.201806017

Yang JX (2020) Study on the superficial characteristics and rock-forming processes and ore-forming processes of the Maoniuping Rare Earth Deposit in Western Sichuan. University of Chinese Academy of Sciences, China. https://doi.org/10.27544/d.cnki.gzcds.2020.000044

Zhang YY, Huang ZQ, Zhao F, Yuan GX, Wang HJ, Ran T (2022) Study on Correlation between Mineral Composition and Permeability Characteristics of Weathered Granite. Journal of North China University of Water Resources and Electric Power (Natural Science Edition) 43(1): 103-108. https://doi.org/10.19760/j.ncwu.zk.2022014

Zheng B, Li LD (2015) The Exploring Effect Comparison of Different Settings in Resistivity Tomography. Chinese Journal of Engineering Geophysics 12(1): 33-39. https://doi.org/10.3969/j.issn.1672-7940.2015.01.007

Zhou MF, Li XX, Wang ZC, Li XC, Liu JC (2020) The genesis of regolith-hosted rare earth element and scandium deposits: Current understanding and outlook to future prospecting. Science Bulletin 65(33): 3809-3824. https://doi.org/10.1360/TB-2020-0350